Inorganic Materials, Vol. 40, Suppl. 1, 2004, S33–S49.

Carbon–Carbon Composite Materials

Yu. S. Virgil'ev and I. P. Kalyagina

Research Institute of Structural Graphite Materials, Elektrodnaya ul. 2, Moscow, 111524 Russia

Abstract—Data are summarized on the performance characteristics and properties of Russian-produced and foreign carbon–carbon composite materials for various engineering applications. The effect of neutron irradiation on their macroscopic properties and structure is examined. The relationships between the radiation-induced dimensional changes and properties of the composites are established, which can be used in assessing the engineering performance and optimizing the fabrication of carbon–carbon composites.

INTRODUCTION

Composite materials consisting of reinforcing agents embedded in a matrix are widely used in various applications. There is a large class of materials made up of carbon components: carbon–polymer (PUM), carbon–graphite (GSP), graphite–graphite (ER), siliconized, and carbon–carbon composite materials (CCCMs). The composites of the last group are composed of reinforcing carbon fibers and carbon or graphite matrices produced via several impregnation and pyrolysis cycles. CCCMs combine high mechanical strength, low thermal expansion, increased fracture toughness, good thermal conductivity, and high thermal stability.

The superiority of the CCCMs over other structural materials is particularly clear if one compares the ratios of the tensile strength to density (J):

Material	J, MPa m^3/kg
MPG	0.022
SU-2500	0.037
USB-15	0.50
KUP-VM	0.50
Carbon fiber	1.1–1.7
Steel	0.14

CCCMs are used in the radiochemical industry and are potentially attractive for use in units of nuclear and fusion power plants and high-flux accelerators. They are also potential candidates for use in MHTGR high-temperature control rods.

In this paper, we summarize the available data on the properties of Russian-produced and foreign CCCMs and their variations under neutron irradiation.

CHARACTERIZATION TECHNIQUES

The performance of graphite materials is determined by a set of characteristics listed in the specifications described in [1], which also specify sample dimensions, testing procedures, and irradiation conditions.

Properties of graphite are commonly determined using standard cylindrical samples 6 mm in diameter and 40 mm in length. Since CCCMs have a layered structure, they are tested using prismatic samples with a cross-sectional size several times larger than the fiber length.

First, we used nondestructive techniques to determine the linear dimensions l, weight m, density d, electrical resistivity ρ, dynamic modulus of elasticity E (ultrasound velocity measurements), and linear thermal expansion coefficient α of standard or prismatic samples. Next, each sample was tested in three-point bending to determine the bending strength σ_b. The two halves of the sample were then used to prepare specimens 8 mm in height, which were polished and examined by microstructural analysis. One of the specimens was used in room-temperature steady-state thermal conductivity (λ) measurements and the other was tested in compression (σ_c). The rest of the sample was ground, and the resultant powder was used to determine structural characteristics (c cell parameter, c-axis (L_c) and in-plane (L_a) crystallite dimensions, and degree of graphitization γ) by x-ray diffraction.

Thermal expansion was measured in the range –196 to 20°C, with subsequent revaluation to the range 20–200°C using the formula $\alpha_{200} = 1.14(\alpha_{20} + 0.7 \times 10^{-6})$ [2].

The content of mineral impurities (ash) was determined by burning graphite samples at 900°C in air. We also determined the boron content of the ash.

Consecutive property measurements on the same sample reduce the effect of graphite inhomogeneity on the measurement results.

The above set of properties was used to estimate the radiation resistance of CCCMs as described in [3], which was then determined more accurately in radiation tests.

Irradiations were performed in various reactors [4] using, for the most part, prismatic samples 40 mm in

0020-1685/04/4001-S0033 © 2004 MAIK "Nauka/Interperiodica"

Table 1. Properties of carbon fibers [8]

Fiber	d, g/cm^3	σ, GPa	E, GPa
Grafil-HM	1.90	2.35	403
Modmor-I	1.80	2.82	270
Tornel-75	1.86	2.62	520
Grafil-HT	1.74	2.84	280
Modmor-II	1.76	2.45–3.15	245–315
Toreica-T300A	1.76	2.50	220
Tornel-400	1.78	2.98	210

length. To irradiate carbon fibers, a bundle of fibers 7–17 μm in diameter was placed in a graphite cell, which was then enclosed in an ampule and mounted in place of a standard fuel rod.

In studies by Russian researchers, passive tests are typically used: after irradiation to a preset dose, the samples are withdrawn from the reactor and are characterized as described above. Irradiation–characterization cycles are repeated until a preset neutron fluence is accumulated. The results thus obtained were shown to be identical to those obtained by in situ measurements [5].

The irradiation temperature was monitored by Chromel–Alumel (<700°C), Pt/Pt–Rh (700–1400°C), and W/Re (>1500°C) thermocouples. If thermocouples could not be mounted in the reactor, we used diamond or silicon carbide indicators [6]. This method is based on the steplike variation of the lattice parameter a of irradiated diamond (or silicon carbide) with annealing temperature: a remains unchanged during annealing below the irradiation temperature and returns to its initial level above the irradiation temperature.

Neutron fluences were also determined using silicon carbide and diamond powder indicators [7]: at relatively low irradiation levels, the increase in their lattice parameter is proportional to the neutron dose. In what follows, all fluences are converted to $E > 0.18$ MeV neutron fluences.

CARBON FIBERS

Fabrication and properties. Carbon fibers play a key role in determining the mechanical strength and other properties of composite materials. The properties of fibers and, hence, their irradiation behavior depend on the raw materials (viscose, poly(acrylonitrile) (PAN), or mesophase pitches) and fabrication procedure (particularly, heat-treatment temperature).

The grades of carbon fibers that are produced on a commercial scale are listed in Table 1 [8]. Carbon fibers are, most frequently fabricated from PAN and mesophase pitch (P-25, P-30, and P-55). The latter fibers have a higher modulus of elasticity and thermal conductivity. In Russia, VMN-4 PAN-derived fibers and related carbon cloth are used more widely. The characteristics of VMN-4 along the fiber axis are as follows [9]:

Density	1.65–1.85 g/cm^3
Tensile strength	200–300 MPa
Modulus of elasticity	250–350 GPa
Thermal conductivity	135–350 W/(m K)

Carbon fibers consist of a low-perfection core, similar in structure to glassy carbon, and a structurally perfect, textured shell, formed by graphite layers similar to those in pyrolytic graphite, with their basal planes parallel to the fiber axis and their c axes lying in radial directions.

It is of interest to examine the effects of processing temperature and irradiation on the structure and properties of fibers. This issue has been addressed in only a limited number of studies. Ponomareva and Virgil'ev [10] assessed the effect of heat-treatment temperature on the characteristics of the Russian commercial PAN-derived grades VMN-4 and VPR-19.

To this end, semifinished fibers were heat-treated at temperatures from 1300 to 2800°C. After heat treatment, the following characteristics of the fibers were determined:

lattice parameters a and c, dimensions of coherent scattering domains L_c and L_a, and texture index β (by x-ray diffraction);

density d (in a gravimetric column);

resistivity ρ;

tensile strength σ of individual fibers;

dynamic modulus of elasticity E (from the frequency of bending vibrations of a cantilevered fiber, measured with a He–Ne laser);

fiber diameter D (by laser beam diffraction).

The data in Table 2 demonstrates that, with increasing processing temperature, the fiber structure changes from turbostratic (disordered) to crystalline (ordered). The degree of ordering achieved by heat treatment depends on the fiber structure and is lower (at the level of glassy carbon) in Rayon fibers (poorly graphitizable viscose fibers) [11].

The highest degree of ordering, close to that in pyrolytic graphite, was achieved in P-55 pitch fibers [11] (Fig. 1). Note that glassy carbon and pyrolytic graphite can be regarded as modeling the structural zones of carbon fibers.

Improvements in the structural perfection of carbon fibers are accompanied by changes in their physical properties, similar to those in the properties of pyrolytic graphite in the (001) plane: an increase in d, λ, and E and a decrease in ρ and α. Naturally, the density and thermal conductivity of carbon fibers are lower and their electrical conductivity is higher than those of pyrolytic graphite because of the low degree of ordering in their core.

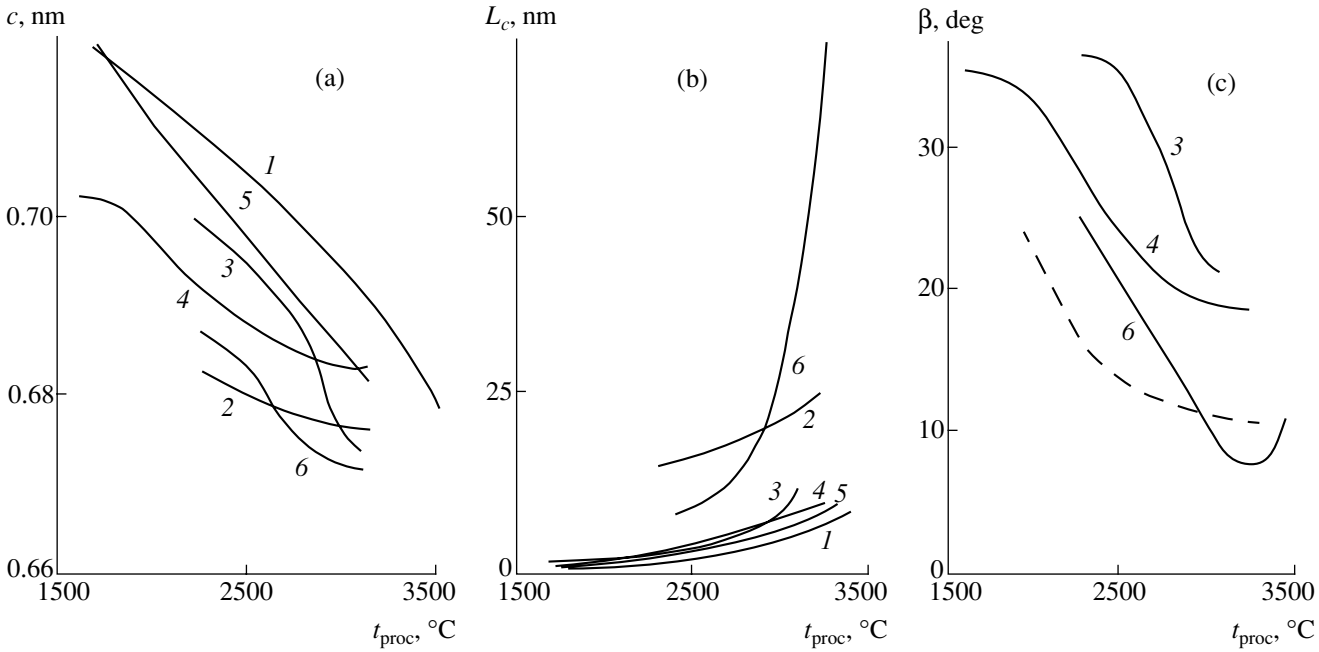

Fig. 1. (a) Lattice parameter c, (b) c-axis crystallite size L_c, and (c) texture index β as functions of processing temperature for (*1*) Rayon, (*2*) P-55, (*3*) VPR, and (*4*) VMN-4 carbon fibers, (*5*) glassy carbon, and (*6*) pyrolytic carbon.

The along-axis values of thermal conductivity reported by Bowers and Sopp [12] for carbon fibers are listed below:

Fiber	K-321	P-25	P-55	P-100	P-120	P-130
λ, W/(m K)	20	22	120	520	640	1100

The characteristics of carbon fibers can be improved by applying coatings. Ponomareva and Virgil'ev [10] reported the characteristics of PAN-derived fibers coated with pyrolytic graphite via heat treatment at 950°C for 150 h. This processing slightly increased the density of the fibers, markedly increased their modulus of elasticity and thermal conductivity, and reduced their thermal expansion.

Effect of neutron irradiation on the properties of carbon fibers. The effect of low-temperature irradiation on the structural properties of VMN-4 and VPR-19 fibers heat-treated between 1300 and 2800°C is similar to that for graphite materials: the c parameter increases, and the crystallite dimensions and texture index decrease. The decrease is larger in more perfect fibers. Raising the irradiation temperature to 400°C reduces these effects [13, 14].

In contrast, high-temperature (1800–2000°C) irradiation improves the structural perfection of fibers: the texture index and c decrease, while the crystallite dimensions increase. This effect is more pronounced in less perfect carbon fibers (Table 3).

Table 2. Characteristics of the fibers studied in [10]

No.	Fiber	t_{proc}, °C	d, g/cm^3	c, nm	a, nm	L_c, nm	L_a, nm	β, deg	E, GPa	σ, GPa	ρ, μΩ m
1	VPR-19	1300	1.72	0.703	0.244	1.6	5.9	38.0	135	1.16	18.3
3		2000	1.80	0.701	0.242	1.9	6.7	34.4	174	3.15	13.1
5		2400	1.85	0.694	0.244	2.3	12.7	27.5	177	2.05	10.1
7		2800	2.01	0.675	0.244	16.8	31.5	21.3	465	1.59	4.4
2	VMN-4	1700	1.67	0.703	0.242	1.9	6.5	37.7			
4		2100	1.67	0.689	0.244	3.4	24.5	26.2			
6		2500		0.686	0.244	5.6	25.5	20.7			
8		3000		0.681	0.245	8.2	35.5	18.0			
9	VMN-4*	1800	1.67	9.696	0.244	2.6	15.0	26.0			

* Commercial batch.

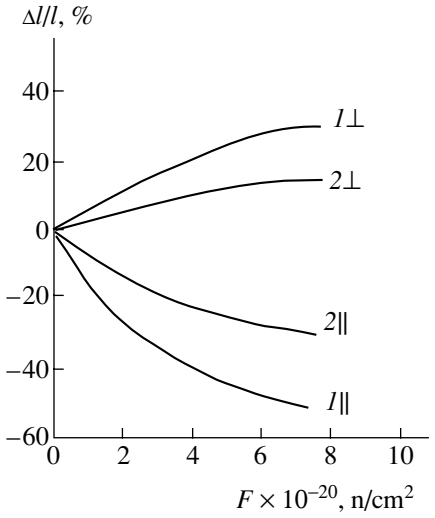

Fig. 2. Radial (⊥) and axial (||) relative size changes vs. neutron fluence for (*1*) Fortafil 5-T, (*2*) Fortafil 3-T, Modmor, and Tornel 300 fibers.

Low-temperature irradiation causes both axial and radial shrinkage of carbon fibers, in contrast to pyrolytic graphite, which experiences *c*-axis swelling. The likely reason is the weight loss caused by radiolytic corrosion. Probably, irradiation to high neutron doses in the absence of corrosion will lead to radial swelling.

The reduction in volume leads to an increase in density, which reduces the increase in resistivity and increases the strength gain. At the same time, the reduction in the modulus of elasticity points to microcracking (Table 3).

High-temperature irradiation of carbon fibers gives rise to axial shrinkage. At the same time, the samples heat-treated above 2000°C undergo radial swelling, and their strength drops. The modulus of elasticity was found to drop only after heat treatment at 2800°C.

The effect of structural perfection on the irradiation behavior of carbon fibers was analyzed by Burchell [11], who irradiated high-perfection pitch fibers prepared at 3100°C (P-55) and less perfect fibers (Rayon) to a high neutron fluence (5×10^{21} n/cm^2) in the range 450–650°C. At 550°C, P-55 experienced a near-zero axial shrinkage, similar to the high-perfection pyrolytic graphite UPV-1T [15], whereas the shrinkage of Rayon (about 7%) was close to that of glassy carbon [16].

During irradiation at 1070°C to a fluence of 7×10^2 n/cm^2, PAN-derived fibers undergo rapid radial swelling (followed by stabilization) and, accordingly, axial shrinkage. Under these conditions, the dimensional changes of Fortafil 5-T highly anisotropic, high-modulus fibers are approximately twice as large as those of the high-strength fibers Fortafil 3-T, Modmor, and Tornel 300 [17] (Fig. 2).

These data, though limited, demonstrate that the radiation-induced dimensional changes in carbon fibers are anisotropic and depend primarily on the structural perfection and modulus of elasticity of the fibers. The shrinkage of low-perfection fibers is close to that of glassy carbon, which models the fiber core. The shrinkage of structurally perfect fibers is much higher and approaches the in-plane shrinkage of pyrolytic graphite, a model material for the fiber shell. Among various carbon materials (pyrolytic carbon, glassy carbon, graphite, and others), carbon fibers experience the highest radiation-induced strain.

CARBON MATRICES

Reinforcing carbon-fiber skeletons are subjected to one or several impregnation (occasionally, under pressure) and/or pyrolysis steps. The resulting matrices may consist of fully isotropic (pitches, tars, and pyrolytic carbon) and/or anisotropic (pyrolytic graphite) carbon materials.

Accordingly, the matrices of CCCMs differ widely in properties, particularly in structural perfection, which is known to play a key role in determining the rate and magnitude of radiation-induced changes in the properties of the matrix and, especially, dimensional changes.

Table 3. Relative changes (%) in the properties of fibers upon irradiation (fluence *F*)

No.	t_{irr}, °C	$F \times 10^{-20}$, n/cm^2	$\Delta l/l$	$\Delta D/D$	$\Delta V/V$	$\Delta d/d$	$\Delta\rho/\rho$	$\Delta\sigma/\sigma$	$\Delta E/E$
1	50–90	2.4	–3.1	–6.7	–10	1.6	733	–52	–11
5		4.8	–3.4	–27	–49	2.3	308	46	–37
7		4.8	–2.6	–23	–42	16.8	185	485	–46
3	1800–2000	1–2	–3.3	–7.5	–17	3.43	–52	–66	42
5		1–2	–6.9	2.7	–2	3.75	–24	–32	45
7		1–2	–1.8	17.3	+35	1.94	20	–74	–52

Note: The same sample numbers as in Table 2.

Figure 3 shows the dose dependences of relative size changes for isotropic carbon materials modeling the matrix:

pitch-based synthetic graphite (GP) [18, 19];

phenol–formaldehyde resin (SU) [17, 20];

bulk pyrolytic carbons with densities of 1.55 [15] and 1.87 g/cm^3 [17].

The pitch-coke-based graphite is seen to undergo the lowest shrinkage (2–3%) both at 400–500 and 1000–1100°C. Nongraphitized glassy carbon experiences a shrinkage of 8–9%, independent of temperature, and exhibits no secondary swelling up to a fluence of 4.4×10^{22} n/cm^2. During irradiation of low-density pyrolytic carbon at 500°C, a low shrinkage (2.5%) gives way to secondary swelling at a fluence of 4×10^{21} n/cm^2. At 1070°C, the secondary swelling of perpendicular samples of dense pyrolytic carbon begins at lower doses. Parallel samples experience a shrinkage of up to 8% upon irradiation to a fluence of 10^{22} n/cm^2.

Thus, the size changes in matrices range widely. Therefore, the matrix and reinforcing carbon fibers must adhere tenaciously to each other and must be close in the rate of dimensional changes. Otherwise, the fibers will debond from the matrix.

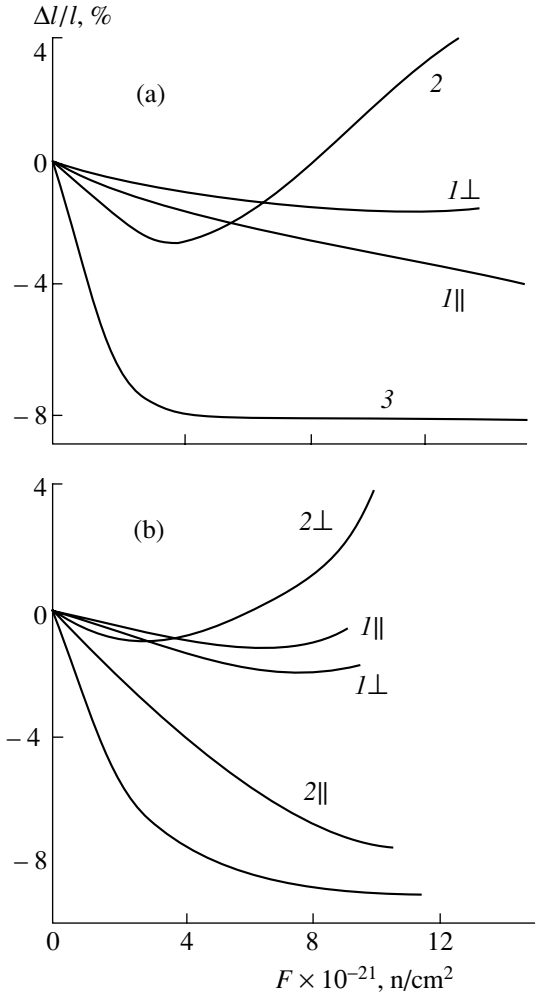

Fig. 3. Relative size changes vs. neutron fluence for different matrix materials irradiated at (a) 400–500 and (b) 1070°C: (*1*) synthetic graphite based on pitch coke, (*2*) pyrolytic carbon; (*3*) glassy carbon; samples cut parallel (||) and perpendicular (⊥) to the block axis.

CARBON–CARBON COMPOSITE MATERIALS

CCCMs are poorly ordered materials with a low degree of graphitization, which have a rather complex structure: a skeleton built from high-modulus or high-strength anisotropic fibers (or cloth) reinforces an isotropic carbon matrix. This heterogeneous microstructure ensures a high mechanical strength but presents problems under irradiation since the matrix and fibers differ in radiation-induced size changes.

The manufacture of CCCMs involves the fabrication of the skeleton via winding, stacking, assembly, or other methods and the preparation of a carbon matrix by carbonizing binders or depositing pyrolytic carbon in pores, followed by heat treatment. To obtain dense materials, impregnation–carbonizing cycles are repeated several times [21].

There are a great number of CCCMs, widely differing in performance characteristics. The properties of some foreign CCCMs are listed in Table 4 [22, 23], and those of the Russian-produced composites KM5415 and KUP-VM-2 are listed in Table 5 [24, 25].

Below, we describe the characteristics of some commercial CCCMs differing in structure and irradiated under different conditions [26–29].

TKM (0D): material reinforced with chopped fibers;

KUP-VM (1D): unidirectional material based on VMN-4 PAN-derived fibers, with a matrix prepared from bakelite lacquer, phenolic resin, and pyrolytic carbon;

KP-14 (2D): 2D-reinforced material based on low-modulus cloth impregnated with pyrolytic carbon and phenol–formaldehyde resin;

UPA-3 (2D): a pyrolytic graphite matrix 2D-reinforced with VMN-4 fibers;

UPA-4 (3D): a pyrolytic graphite matrix 3D-reinforced with VMN-4 fibers;

3KUM-P (3D): a matrix 3D-reinforced with VMN-4 fibers;

4KMS (4D): a 4D-reinforced matrix produced by multiple pitch impregnations of a skeleton;

Termar-TD (2D): layers of TGN-2M carbon cloth alternating with layers of chopped VPR-19 fibers, bound by coal-tar pitch and pyrolytic carbon;

Dakum (2D): 2D-reinforced material consisting of URAL pyrocarbon-coated carbon cloth and a matrix composed of cokes (heat treatment of coal-tar pitch and

Table 4. Properties of some foreign CCCMs [22, 23]

Manufacturer	Composite	d, g/cm^3	σ_t, MPa	σ_b, MPa	σ_c, MPa	E, GPa
Across	AC 250	1.7		540	235	
Comp., Ltd.	AC 200	1.7		145	95	
	AC 100	1.7		75	75	
HITCO Carb.	Chemcarb*	1.8	275	305	210	125
Composites		1.8	225	225	165	70
		1.8	70	110	75	20
SGL Carbon	Sigrabond					
Group	1501G	1.5	320–400	250–300		
	1601G	1.4	300–350	150–200		
	1001G	1.4	55–65	28–33		
	A05	1.7	54			17–22
			9			
Toyo Tanso Co.	CX 2002U	1.55	35		50	8–11
			11		54	3.4

* Different winding angles of fibers.

phenol–formaldehyde resin at 2100°C) and pitch (heat treatment at 1000°C);

Grauris (3D): 3D-reinforced material consisting of URAL cloth die-pressed in the third direction and a matrix prepared from phenol–formaldehyde resin and low-temperature (1000°C) pyrolytic carbon;

Desna 4 (4D): a 4D-reinforced composite based on UKN-5000 fibers, with a matrix prepared via multiple pitch-impregnation cycles;

Karboksilar (2D): nongraphitized material based on carbon cloth containing ≤10% Si;

FEBUS (2D): 2D-reinforced material based on carbon cloth with incomplete silicon carbonization.

In addition, we tested a number of composites differing in density and final heat-treatment temperature.

The room-temperature properties of the CCCMs are summarized in Table 6. The composites are seen to be anisotropic materials with a low structural perfection and thermal expansion. Their density and other macroscopic properties range widely and, hence, can be controlled by varying the components of the CCCM, heat-treatment temperature, impregnants, and forming pressure and also by doping and thermomechanical processing. The last approach makes it possible to vary the anisotropy of the material.

In addition, there are a number of prototype CCCMs (e.g., UAM) [30] designed for ITER power reactors. The matrices of such CCCMs are produced from pyrolytic carbon densified by pitch impregnations and synthetic resins. Their characteristics are listed in Table 7.

With increasing measurement (working) temperature, the strength of composites increases, in contrast to that of metals (e.g., molybdenum and titanium), alloys, and carbides, which decreases with increasing temper-

Table 5. Characteristics of 2D-reinforced composites for electrical heaters and structural elements of electrical furnaces [24, 25]

Composite	KM-5415	KUP-VM-2*
Density, g/cm^3	1.25	1.35
Strength, MPA		
compression	100	200
bending	150	550
tension	70	370
shear	20	–
Thermal conductivity along (numerator) and across (denominator) the warp, W/(m K)	7.5/4.4	23/2.9**
Resistivity, μΩ m	40	80/17**
Thermal expansion, K^{-1} (20–2000°C)	3.1×10^{-6}	3.0×10^{-6}
Maximum dimensions, mm	$1000 \times 550 \times (3–10)$	

* Unidirectional winding of fibers.

** Winding angle of 75°.

Table 6. Characteristics of commercial CCCMs [26–29]

Composite	t_{proc}, °C	d, g/cm^3	c, nm	σ_c, MPa	σ_b, MPa	E, GPa	$\alpha \times 10^6$, K^{-1} (77–300 K)	λ, W/(m K)	r, μΩ m
TKM	2100	1.45	0.674	110/130	47–65	12–17	0.73	74.7/18.6	10
KUP-VM	2000	1.40	0.676	140/320	240	135	–0.5/5.6	24/1.7	14
KP-14	2600	1.45	0.673	72/131	71	15	1.4/3.8	8.5/4.2	
UPA-3	2100	2.00	0.683	20/40	14.5	5.8	1.3	138/18	
UPA-4	2100	1.40	0.686	68/75	55/36	9.5	3.0/2.5	6.8/3.9	49
3KUM-P	2150	1.9	0.679	67/58	10	35/22		55/50	26
4KMS	2200	1.9	0.674	148	29	45	1.0	49	18
Termar-TD	2000	1.65	0.674	110/130	–/80	–/4.6	0.73/2.5	67/23	12/38
Dakum	1600	1.37	0.683	–/120	110/8	22/8	2.3/3.0	12/3.2	45/110
Dakum	2000	1.40	0.685	–/90	135/10	14/6	1.2/2.7	12/3.4	40/100
Grauris	1800	1.25	0.687	90	120	19	–	–	45
Karboksilar	1000	0.98	0.683		100	7/–	1.2/3.3	3.1/1.2	97
FEBUS	1900	2.70		200	120	53	3.0	15	
Desna 4	2150	1.90	0.678	70	90	30	1.0	70	16

Note: Samples cut along (numerator) and across (denominator) the layers; average values for isotropic materials and also along the weft and warp.

Table 7. Characteristics of CCCMs irradiated in the BOR-60 reactor [30]

Composite	Reinforcing agents	t_{proc}, °C	d, g/cm^3	σ_c, MPa	E, MPa	$\alpha \times 10^6$, K^{-1} (77–300 K)	ρ, μΩ m	λ, W/(m K)
UAM-3D	UKN-5000 fibers	1000	1.56–1.62	–	33/18	0.6/0.8	37/73	–
UAM-92-3D-Gr	Fibers + granite	2800	1.83–1.87	150	–	0.5	–	360
UAM-92-5D-Gr	Fibers + granite	2800	1.83–1.87	105/–	–/26	0.5/0.2	–/26	425/–
TGN-2M	TGN-2MB cloth	1000	1.44	–	23/–	2.9/–	38/–	–/–
TKM	UKN-5000 fibers	2100	1.83	–	22	–0.1	10	54/23
Desna	UKN-5000 fibers	2150	1.86	70	30	1.0	16	70

Note: Samples cut along (numerator) and across (denominator) the layers.

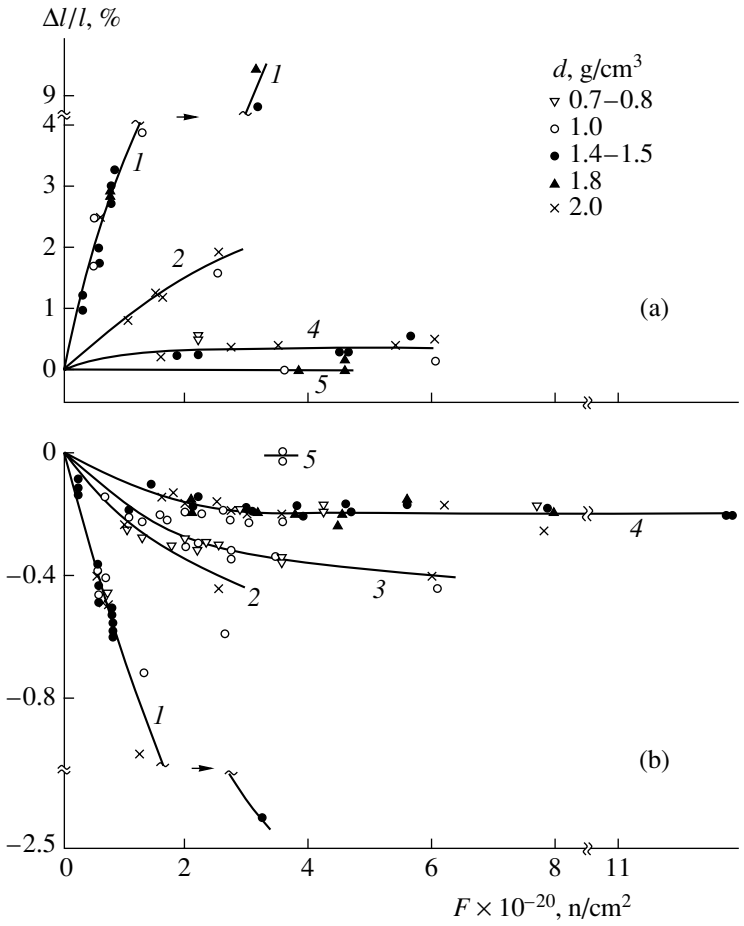

Fig. 4. Relative size changes vs. neutron fluence for TKM (0D) samples differing in density; irradiation at (*1*) 50–90, (*2*) 100–140, (*3*) 250–300, (*4*) 400–500, and (*5*) 700–800°C; samples cut (a) across and (b) along the fiber layers.

ature and, above approximately 1200°C, is lower than the strength of composites.

Irradiation effects on the properties of CCCMs. Irradiation-induces dimensional changes play a key role in determining the variation in the performance of reactor components.

The dose dependences of dimensional changes in the 0D-reinforced composite TKM between 50 and 950°C are illustrated in Fig. 4. Irradiation at 50–90°C gives rise to rapid expansion of samples across the fiber axis and shrinkage along the fiber axis, but the sample dimensions stabilize at relatively low doses. The dimensional changes sharply decrease with increasing temperature and are close to zero at 700–800°C. The data points for different densities (from 0.7 to 2.0 g/cm^3) fall on different curves. High neutron fluences (5.4×10^{21} n/cm^2) at 400°C give rise to swelling of perpendicular samples (≤1.2%) and shrinkage of parallel samples (≤1.1%) [30].

Irradiation of the unidirectional composite KUP-VM (Fig. 5) leads to a significant shrinkage along the fiber axis and swelling across the fiber axis. The rate of dimensional changes decreases with increasing irradiation temperature. Above 350°C, the material undergoes shrinkage in the two directions; the shrinkage begins at lower neutron fluences, and its rate increases with temperature. At 1000–1100°C, shrinkage begins at higher fluences, and the shrinkage rate continues to rise.

Similar behavior is exhibited by the 2D-reinforced composite Termar: expansion across the fibers and a significant shrinkage along the fibers. The rate of dimensional changes decreases with increasing irradiation temperature. Above 350°C (up to at least 1400°C), the shrinkage rate along the fibers is independent of the irradiation temperature. Irradiation with a fluence of 3×10^{21} n/cm^2 leads to a shrinkage of 4% [29].

The presence of silicon carbide in the nongraphitized material Karboksilar sharply reduces the irradiation-induced shrinkage, to the level of silicon carbide (no more than 1%) [31]. Low-temperature (50–90°C) irradiation with a fluence of 10^{21} n/cm^2 causes a very low isotropic shrinkage. At 1400°C, the shrinkage rate is also slow: at a fluence of 0.8×10^{20} n/cm^2, the shrinkage does not exceed 0.8% [32]. Since FEBUS has a similar structure. it may be expected to exhibit similar behavior.

At high temperatures (800–1000°C) and fluences (up to 7.5×10^{20} n/cm^2), the swelling rate of perpendicular TKM samples is close to that of pyrolytic graphite, and the swelling attains 37%. Termar experiences a smaller swelling, and KUP-VM undergoes a shrinkage of 11%.

The shrinkage rate of Termar samples cut along the fiber axis is close to those of pyrolytic graphite and glassy carbon. At the same time, the shrinkage rate of parallel KUP-VM and TKM samples is faster by a factor of 2, and the shrinkage attains 20% at a fluence of 6.5×10^{20} n/cm^2.

Figure 6 compares the dimensional changes in UAM 3D–5D composites (Table 7), Desna (3D), and TKM (0D) irradiated with high fluences in the BOR-60 at 400°C. Also included are the data points shown in Fig. 4 for TKM irradiated at the same temperature. It can be seen that the presence of low-temperature pyrolytic carbon in the matrix of the UAM composites leads to a high anisotropic shrinkage. The shrinkage of the samples cut perpendicular to the block height is lower and does not depend on the nature (structure) of the material. The shrinkage of parallel samples attains 12%, with a significant scatter of data points. TKM and Desna are far more stable: after irradiation with a fluence of 6.8×10^{21} n/cm^2, the maximum longitudinal shrinkage of the latter does not exceed 1.6% [30].

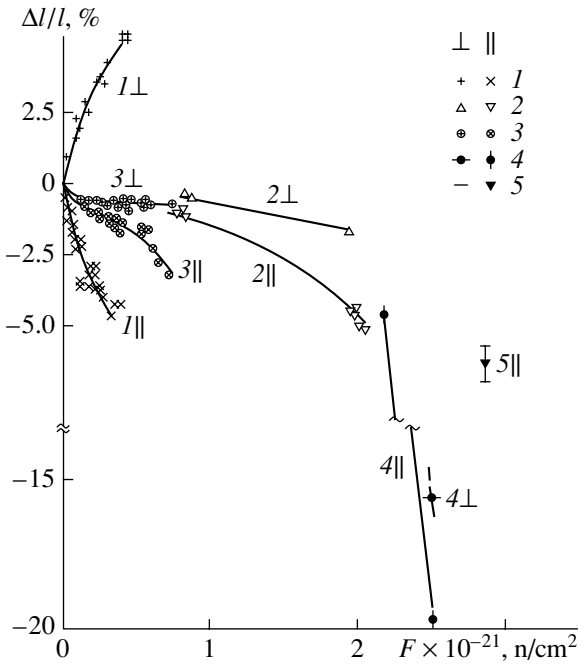

Fig. 5. Relative size changes vs. neutron fluence for KUP-VM irradiated at (*1*) 50–90, (*2*) 300, (*3*) 400–500, (*4*) 1000–1100°C, and (*5*) 1400°C; samples cut along (∥) and across (⊥) the fiber axis.

During high-fluence irradiation at temperatures of up to 1000°C [30, 33], the shrinkage of UAM-92-5D tends to decrease and give way to swelling in the two directions. The accompanying changes in physical properties are, however, inconsistent with secondary swelling:

t_{irr}, °C		400	600	600	800	1000	1000
$F \times 10^{-21}$, n/cm^2		4.6	4.1	7.2	4.6	5.7	10
$\Delta l/l$, %	∥	–12	–0.7	–0.3	–4.0	2.0	2.2
	⊥	–2.3	1.9	0.9	3.9	4.0	5.2

Irradiation of UPA-4, Dakum, Grauris, and Karboksilar at "emergency" temperatures (1800°C) to a fluence of 10^{20} n/cm^2 causes a shrinkage no higher than 1% [28].

Table 8 summarizes the dimensional changes in five composites irradiated at 500–600°C (four composites containing PAN-derived fibers and one pitch-fiber composite) [34]. 0D- (RFC) and 3D-reinforced samples undergo shrinkage, which is lower than that of the pitch-fiber-reinforced composite. At the same time, the dimensional stability of the 1D- and 2D-reinforced materials is poorer: irradiation with a fluence of 5.3×10^{21} n/cm^2 leads to swelling of these materials. Raising the temperature to 800°C and the fluence to 7.8×10^{21} n/cm^2 slightly reduces (to 1.5%) the shrinkage of the pitch-fiber composite along the three directions, without swelling. The shrinkage of the samples under consideration is of the same order as that of the Russian-produced materials TKM and Desna after irradiation under similar conditions.

Table 8. Effect of the reinforcement level on the size changes in RFC samples irradiated at 500–600°C [34]

Fibers	PAN	PAN	PAN	PAN	Pitch
Reinforcement level	0D	1D	2D	3D	3D
$\Delta l/l$, % (F = 1.6 dpa)	–0.4 / –0.4	–1 / –0.1	–1.2 / –0.2	–1.2 / –1.2	–0.8 / –0.7
$\Delta l/l$, % (F = 4.7 dpa)	–2.0 / <–0.5	4.0 / 0.6	2.5 / <–0.5	–3.0 / –2.5	–2.0 / –2.0
$\Delta l/l$, % (F = 7 dpa)					–1.5 / –1.5

Note: Samples cut along (numerator) and across (denominator) the layers; 1 dpa = 1.12×10^{21} n/cm^2.

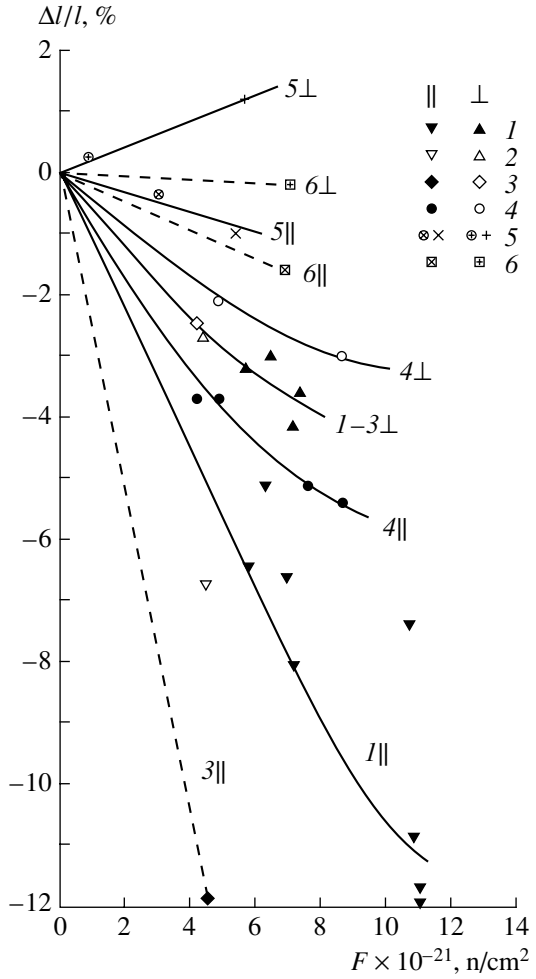

Fig. 6. Relative size changes vs. neutron fluence for (*1*) UAM-3D, (*2*) UAM-92-3D, (*3*) UAM-92-5D, (*4*) TGN-2MB, (*5*) TKM, and (*6*) Desna irradiated in the BOR-60 at 400–500°C; samples cut parallel (||) and perpendicular (⊥) to the block axis.

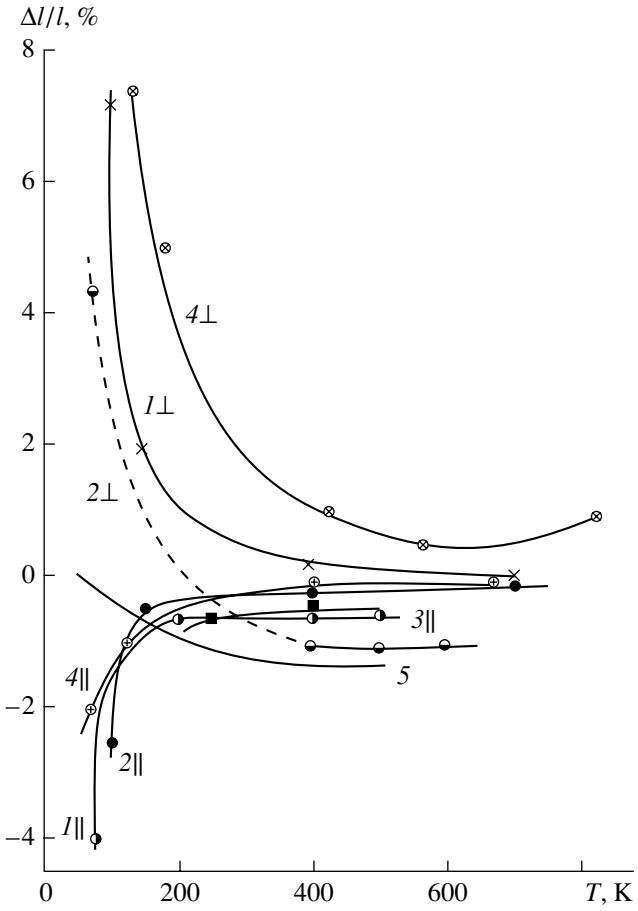

Fig. 7. Relative size changes vs. irradiation temperature for (*1*) TKM, (*2*) KUP-VM, (*3*) 3KUM-P, (*4*) pyrolytic graphite, and (*5*) glassy carbon irradiated to a fluence of 3×10^{20} n/cm^2; samples oriented perpendicular (⊥) and parallel (||) to the basal plane (across and along the fibers, respectively).

The absence of secondary swelling in the samples with a low structural perfection is probably associated with their high strength. Similar behavior was exhibited by nongraphitized glassy carbon under high-fluence irradiation [20].

It follows from the above that the radiation-induced size changes in composites depend on the following factors:

irradiation conditions,

sample dimensions (size effect),

properties of the material (density, thermal expansion, structural perfection, and strength),

components of the material (reinforcing fibers, matrix, and dopants) and interaction between them, and

macroscopic structure (architecture) of the material.

Raising the irradiation temperature sharply reduces both swelling and shrinkage, as illustrated in Fig. 7 for a fluence of 3×10^{20} n/cm^2. Above 400°C, the irradiation temperature has little effect on size changes [30]. At the same time, upon high-fluence (1.1×10^{21} n/cm^2) irradiation of the 2D composites A05 and CX 2002U and the 3D composite N 112 at temperatures above 600°C, the swelling of perpendicular samples and shrinkage of parallel samples increase steadily with temperature (Fig. 8) [35].

As a result of the size effect, the strain in larger samples (10 mm in diameter) was lower than that in smaller samples (5 mm in diameter) [30]. One would expect that the strain in bulk articles, with no disruption of the reinforcement, will be even lower.

Sample density was found to have no effect on the dimensional changes in the 0D-reinforced composite TKM (Fig. 4), since its density was varied via impregnations with a graphitizable pitch.

At the same time, reducing the density of KP-14 by increasing the content (*C*) of shrinking low-density cloth compensates for the swelling of the graphitized-

pitch matrix. As a result, the shrinkage $\Delta V/V$ gives way to swelling [36]:

Density, g/cm^3	1.9	1.6	1.4
C, %	59	71	73
$\Delta V/V$, %	10.0	2.0	–3.0

The effect of heat-treatment temperature on size changes can be illustrated by the example of KUP-VM: increasing the heat-treatment temperature has an insignificant effect on the shrinkage of samples irradiated at 50–90°C with a fluence of 2.7×10^{20} n/cm^2:

Heat-treatment temperature, °C	1000	2000	2800
$\Delta l/l$, %	–3.40	–3.42	–3.45

At the same time, 600°C high-fluence (1.2×10^{21} n/cm^2) irradiation of 3D composites based on fibers heat-treated at 2700°C (P-55 and PAN-derived fibers) led to a volume shrinkage of 1.6% in the former material and 2.7% in the latter (lower structural perfection). Heat treatment of the fibers at 3100°C caused only a slight decrease in shrinkage: to 1 and 2%, respectively [34].

Consider the interaction between the constituents components (reinforcing fibers, matrix, and dopants) of composites. It follows from the above that the effect of the high-strength, anisotropic carbon fibers, which experience large (in comparison with the matrix) dimensional changes, prevails, leading to a shrinkage of the composite along the fibers and swelling across the fibers. To a first approximation, the net effect obeys the additivity rule if there is an adequate adhesion between the components (ensuring the integrity of the composite).

Impregnants influence the structural perfection of CCCMs, contributing to their stability. Well-graphitizable pitches have little effect on radiation hardness, whereas synthetic resins and low-temperature pyrolytic carbon are favorable for the shrinkage of the material. Doping with silicon reduces the radiation-induced dimensional changes.

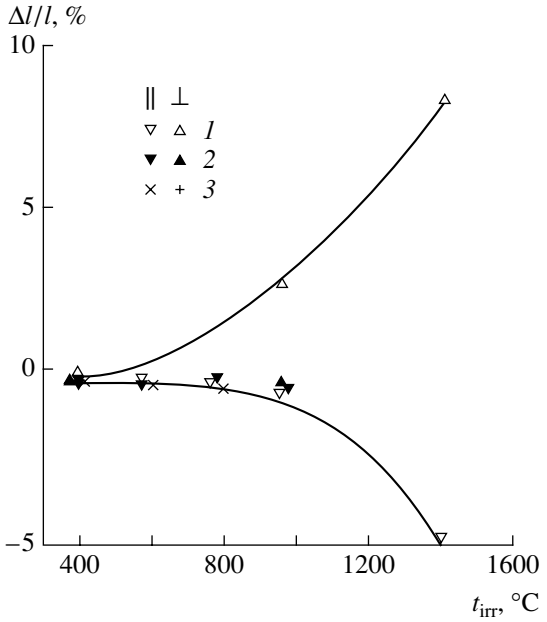

Fig. 8. Relative size changes vs. irradiation temperature for the (*1*) A05, (*2*) CX2002U, and (*3*) N112 composites irradiated to a fluence of 1.1×10^{21} n/cm^2; samples oriented across (⊥) and along (||) the fibers.

The influence of the CCCM architecture on the linear and volume size changes at 50–90°C, the temperature range in which irradiation effects are rather strong even at low neutron fluences, is illustrated in Table 9, which presents data for composites close in structural perfection but differing in reinforcement level. It can be seen that a more complicated architecture of CCCMs leads to more isotropic dimensional changes, causes swelling to give way to shrinkage (owing to the higher fiber content), and slightly reduces the volume shrinkage [36].

As shown earlier [37], the volume shrinkage of CCCMs irradiated at 400–500°C with a fluence of 2×10^{20} n/cm^2 decreases as the material architecture becomes more complex; the volume shrinkage of 4D-reinforced composites is close to zero. Moreover, Burchell *et al.* [34] pointed out that, at 500–600°C, the stability of 1D- and 2D-reinforced composites was

Table 9. Effect of the reinforcement level on the size changes in CCCMs irradiated at 50–90°C with a fluence of 2×10^{20} n/cm^2 [36]

Composite	TKM	KUP-VM	KP-14	UPA-3	UPA-4	3KUM-P	4KMS
Reinforcement level	0D	1D	2D	2D	3D	3D	4D
$\Delta l/l$, %	$\frac{-1.6}{6.0}$	$\frac{-2.5}{3.0}$	$\frac{-3.0}{3.2}$	$\frac{-0.5}{0.8}$	$\frac{-1.0}{0.2}$	$\frac{-0.2}{-0.2}$	$\frac{-1.2}{0.4}$
$\Delta V/V$, %	10.6	3.5	3.3	1.1	–0.6	–0.6	–0.4

Note: Samples cut along (numerator) and across (denominator) the layers.

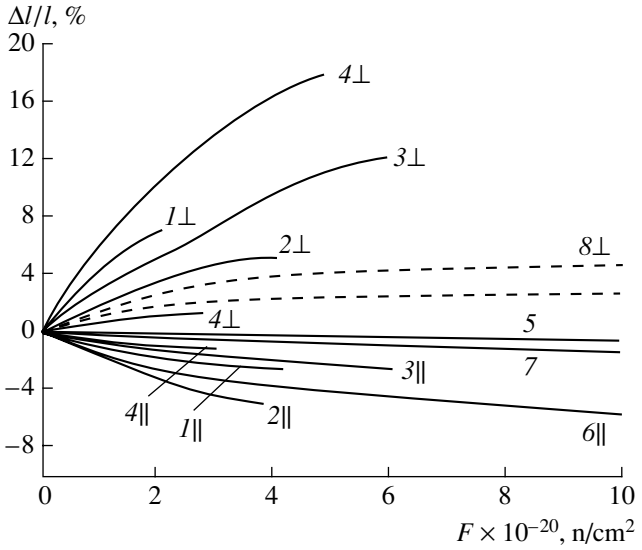

Fig. 9. Relative size changes vs. neutron fluence for (*1*) TKM, (*2*) KUP-VM, (*3*) Termar-TD, (*4*) Dakum, (*5*) Karboksilar, (*6*) pyrolytic graphite, (*7*) glassy carbon, and (*8*) the reactor graphite GR-280 irradiated at 50–90°C; samples cut perpendicular (⊥) and parallel (||) to the preferential orientation of the basal plane (across and along the fibers, respectively).

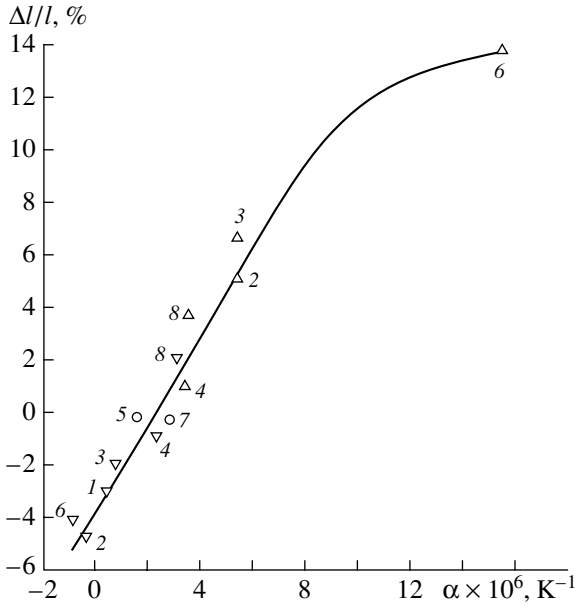

Fig. 10. Correlation between the thermal expansion and size changes of CCCMs and graphite materials irradiated at 50–90°C to a fluence of 3×10^{20} n/cm^2; (*1–8*) same as in Fig. 9.

lower than that of 0D- and 3D-reinforced materials (Table 8).

As in the case of graphite materials, the final strain (Table 6) is proportional to the linear thermal expansion coefficient (Fig. 9). The curve in Fig. 10 includes the data points for pyrolytic graphite and glassy carbon, which are model materials for the fiber core and shell, respectively [15, 20], and also the data point representing the reactor graphite GR-280 [38]. Therefore, to minimize radiation-induced size changes, the composite must be isotropic, with $\alpha = (3–4) \times 10^{-6}$ K^{-1}.

The effects of neutron fluence and irradiation temperature on the physical properties of CCCMs are similar to those for well-studied structural graphite materials. The anisotropy in properties persists after irradiation.

Since the components of CCCMs differ in the rate of radiation-induced size changes, the fibers, having a higher shrinkage rate, may debond from the matrix if the sliding resistance is not high enough. Fiber sliding leads to the formation of pits on irradiated surfaces and cracking along the fibers (Fig. 11a).

The photographs in Fig. 11b illustrate the macroscopic deformation (swelling, bending, and disruption of fibers) of (*1*, *2*) TKM, (*3–5*) KUP-VM, (*6–9*) TGN-2M, and (*10–12*) 3KUM-P irradiated under the following conditions:

t_{irr}, °C		800	–	200	1100	–	350	700	600	–	50	50
$F \times 10^{-21}$, n/cm^2	0	7.3	0	1.6	2.5	0	0.3	2.9	6.2	0	0.1	0.2
Sample no. in Fig. 11b	*1*	*2*	*3*	*4*	*5*	*6*	*7*	*8*	*9*	*10*	*11*	*12*

Irradiation to a fluence of 10^{22} n/cm^2 led to fiber disruption.

According to Lebedev and Pokrovskii [30], irradiation at 400°C with fluences of up to 5×10^{21} n/cm^2 gives rise to macroscopic deformation of UAM-3D and delamination of TGN-2M along the cloth layers. Further irradiation leads to fiber disintegration. At the same time, no fiber disruption occurs in UAM-92-3D and UAM-92-5D.

The thermal expansion of the KP-14 and UPA-4 composites, differing in structural perfection (the latter is less perfect), decreases under any irradiation conditions. The decrease is less pronounced in the case of UPA-4 (Table 10). Similar behavior was observed earlier for pyrolytic graphite [15].

Low-fluence (2×10^{20} n/cm^2) irradiation at 200–620°C causes an insignificant increase in the thermal

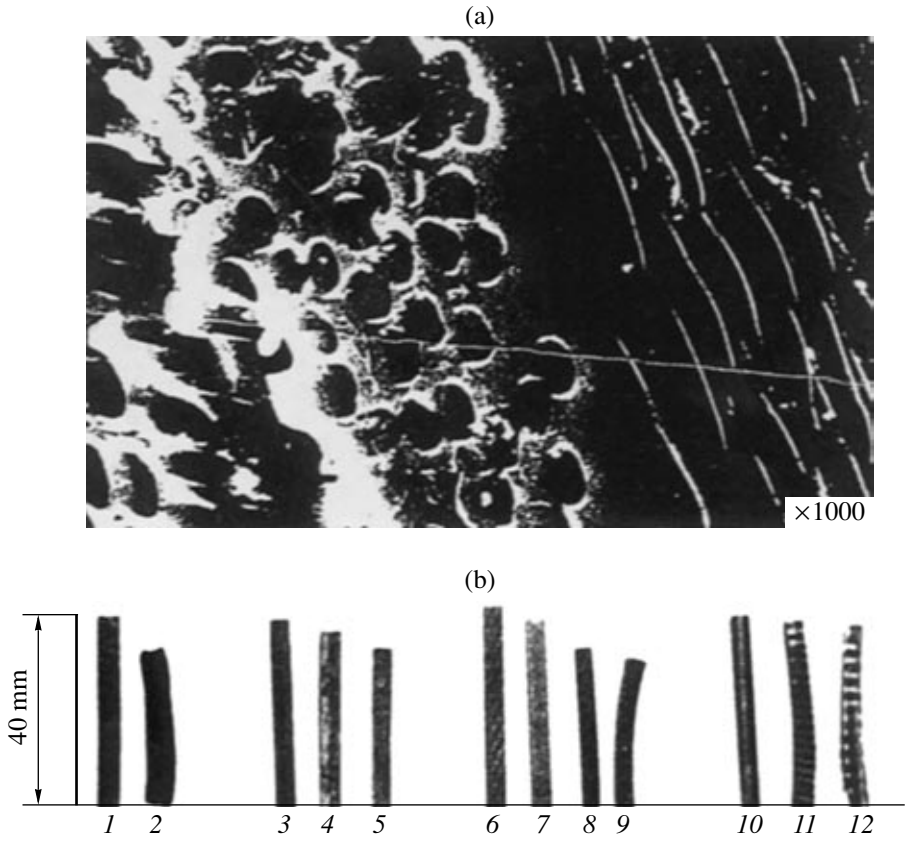

Fig. 11. (a) Micrograph showing a polished surface of KUP-VM after irradiation at 600°C to a fluence of 6.2×10^{20} n/cm^2. (b) Photographs of different composites before and after irradiation under conditions specified in text.

expansion of 3D- and 4D-reinforced UAM composites [39].

Irradiation at 620°C to a fluence of 1.8 dpa increases the thermal expansion of the 3D composite N 112 by a factor of 2.7: from 0.69×10^{-6} to 1.85×10^{-6} K^{-1}. The α/α_0 ratio of A05 and CX 2002U irradiated at 620–1000°C to 0.8–1.8 dpa varies from 0.74 to 1.33, depending on the crystallographic orientation [40].

The α of the composites listed in Table 7 increases upon irradiation at 400°C to fluences above 0.4×10^{22} n/cm^2 [30]. The increase in α grows with fluence, from 50–100 (UAM-92-5D) to 750% (Desna at 1000°C).

The thermal conductivity of CCCMs first decreases rapidly with increasing fluence, as does that of synthetic graphite, and then stabilizes at a level that is positively correlated with the initial thermal conductivity. The relative change in thermal conductivity is independent of its initial value, and the anisotropy in λ persists. At the same time, the composites with a low initial

Table 10. Effect of neutron irradiation on the thermal expansion α of KP-14 and UPA-4

KP-14	t_{irr}, °C		50	50	400	450	450	450	
	$F \times 10^{-21}$, n/cm^2	0	0.7	0.7	4.0	3.8	3.8	6.4	
	$\alpha \times 10^6$, K^{-1}	1.4	–0.12	0	0	–0.25	–1.0	–1.2	
	$\Delta\alpha/\alpha$	0	–1.1	–1.0	–1.0	–1.2	–1.7	–1.9	
UPA-4	t_{irr}, °C		50	300	350	400	600	700	1300
	$F \times 10^{-20}$, n/cm^2	0	1.0	1.8	4.3	4.9	5.4	3.0	20
	$\alpha \times 10^6$, K^{-1}	3.0	1.3	2.5	1.7	1.7	1.6	1.6	1.6
	$\Delta\alpha/\alpha$	0	–0.57	–0.2	–0.4	–0.4	–0.4	–0.4	–0.4

Note: Samples cut along the layers; α in the range 77–300 K.

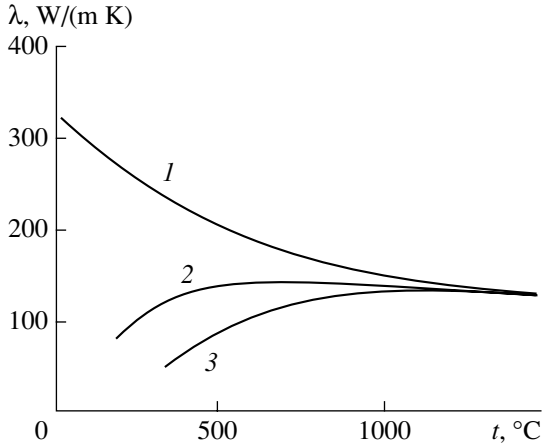

Fig. 12. Thermal conductivity as a function of measurement temperature for a 3D-reinforced composite (*1*) before and (*2*, *3*) after irradiation with fluences of 5.6×10^{19} and 1.1×10^{21} n/cm^2, respectively; measurements at the irradiation temperature.

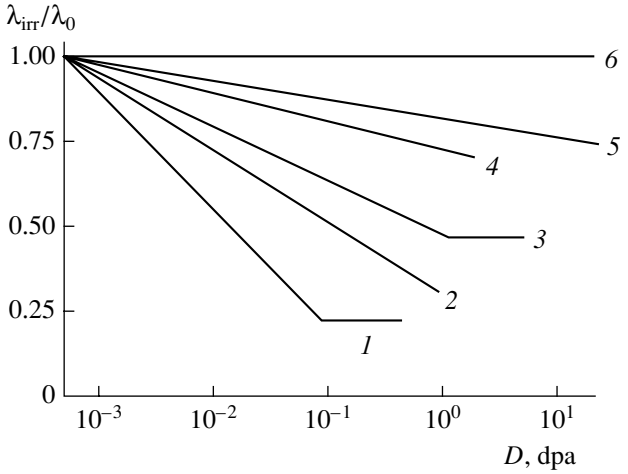

Fig. 13. λ_{irr}/λ_0 ratio as a function of radiation damage for different CCCMs; irradiation and measurements at (*1*) 150–200, (*2*) 370–420, (*3*) 600–620, (*4*) 820, (*5*) 1000, and (*6*) 1500°C.

structural perfection show an increase in λ, rather than a decrease, owing to the increase in the degree of crystallinity [7].

Thermal conductivity is commonly measured at room temperature. With increasing temperature, the thermal conductivity of unirradiated graphite drops, while that of irradiated graphite rises. Starting at about 1200°C, irradiation has no effect on the thermal conductivity of graphite (Fig. 12) [40]. In view of this, Fig. 13 shows the λ_{irr}/λ_0 ratio in different CCCMs as a function of radiation damage for the thermal conductivity at the irradiation temperature.

After irradiation to a fluence of 5×10^{21} n/cm^2, the 1300°C thermal conductivity of the 3D-reinforced composites listed in Table 8 was 60 W/(m K) [34].

It is clear from Fig. 13 that the stabilization level decreases with decreasing irradiation temperature: λ decreases by a factor of 2 at the working temperature (600°C) and remains unchanged at 1500°C.

The effect of neutron irradiation on the thermal conductivity and thermal resistance (inverse of thermal conductivity) of KP-14 and UPA-4 (composites with a low density, $d = 1.4$ g/cm^3, and low thermal conductivity) is illustrated in Table 11. It can be seen that irradiation produces no changes in thermal conductivity to within the measurement accuracy and scatter in the initial thermal conductivity. The $\Delta K/K$ in the composites is close to that in the molded reactor graphite GR-220 [41].

High-fluence irradiation markedly reduces the (initially high) thermal conductivity of UAM-92-5D. The

Table 11. Thermal conductivity (λ) and relative changes in the thermal resistance ($\Delta K/K$) of irradiated KP-14 and UPA-4

KP-14	t_{irr}, °C		50	300	400	450	450	450	600	600
	$F \times 10^{-21}$, n/cm^2	0	0.7	2.3	2.6	3.8	3.8	6.4	6.2	6.2
	λ, W/(m K)	8.5 4.2	3.6 1.2	3.9 0.9	9.3 3.7	15.9 5.7	22.2 3.7	10.0 1.4	4.1 2.9	18.6 3.4
	$\Delta K/K$	0	1.4 2.5	1.2 3.7	–0.1 0.1	–0.5 –0.3	–0.6 0.1	–0.2 2.0	1.1 0.4	–0.5 0.2
UPA-4	t_{irr}, °C		50	50	400	400	450	450	560	560
	$F \times 10^{-21}$, n/cm^2	0	2.2	3.1	3.9	3.9	6.4	6.4	7.3	7.3
	λ, W/(m K)	6.8 3.9	2.0 1.1	1.5 0.8	4.4 2.6	1.6 1.3	5.5 3.9	2.6 1.4	4.7 2.2	1.9 1.3
	$\Delta K/K$	0	2.4 2.5	3.5 3.9	0.5 0.5	3.2 2.0	0.2 0	1.7 1.8	0.5 0.8	2.6 2.0

Note: Samples cut along (numerator) and across (denominator) the layers; room-temperature measurements.

final level of in-plane thermal conductivity depends little on the irradiation temperature [33, 39]:

t_{irr}, °C	–	200	370	400	600	600	1000
$F \times 10^{-20}$, n/cm^2	0	0.8	1.0	44	1.8	72	57
λ, W/(m K)	290	30	95	20	90	30	10

The electrical resistivity of CCCMs, being not a performance parameter, can be used to follow changes in the state of materials. The increase in the resistivity of reactor graphites upon neutron irradiation is at a level of 200% and depends little on the irradiation temperature. The increase in ρ is larger at lower initial values (in well-crystallized materials) and is smaller for disordered materials. The resistivity of nongraphitized, semifinished reactor graphite remains unchanged under irradiation. In addition, Δρ decreases owing to the graphite densification as a result of shrinkage. At the same time, Δρ increases rapidly as secondary swelling develops, because the material becomes looser.

At 50–90°C, the Δρ/ρ of poorly crystallized materials (TKM, KUP-VM) stabilizes at 50%. With increasing irradiation temperature, Δρ/ρ decreases, becoming negative at 1100°C (Fig. 14). Low-fluence (10^{20} n/cm^2) irradiation at "emergency" temperatures (1800–2000°C) reduces the resistivity of UPA, Grauris, Dakum, Karboksilar, and reactor graphite GR, especially at significant shrinkages, which indicates that the reduction in resistivity is associated with the densification of the material [29]. The resistivity of TGN-2M with a matrix of pyrolytic carbon deposited at 1000°C also decreases [30].

At the same time, high-fluence irradiation above 400°C increases the resistivity of UAM-92-5D by 400–640% [33]:

t_{irr}, °C	400	600	1000
$F \times 10^{-21}$, n/cm^2	4.4	4.1	5.7
Δρ/ρ, %	640	410	580

Irradiation at 400 and 800°C with a fluence of 4.6×10^{21} n/cm^2 increases the resistivity of these composites by a factor of 6 [30]. Since the samples experienced no secondary swelling or cracking (Table 7), this effect can be accounted for, at least in part, by the low initial resistivity and densification (due to shrinkage) of the composites.

An essential point is that the samples show no rapid rise in resistivity, which also confirms that no secondary swelling occurred at the fluences in question.

The dynamic modulus of elasticity also first rises to a certain level and then stabilizes. At the same time, the modulus of elasticity of some composites, e.g., KUP-VM, increases by 100–150% and then drops because of debonding and cracking (Fig. 11b). With increasing irradiation temperature, the variation in E becomes more gradual; above 600–700°C, no drop in E occurs because the difference in dimensional changes between the matrix and fibers is insignificant at these temperatures (Fig. 15).

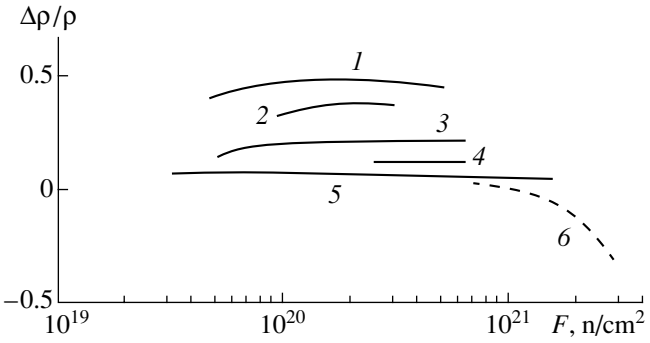

Fig. 14. Relative change in resistivity vs. neutron fluence for KUP-VM irradiated at (*1*) 50–90, (*2*) 300, (*3*) 400–500, (*4*) 700–800, (*5*) 1000, and (*6*) 1100°C.

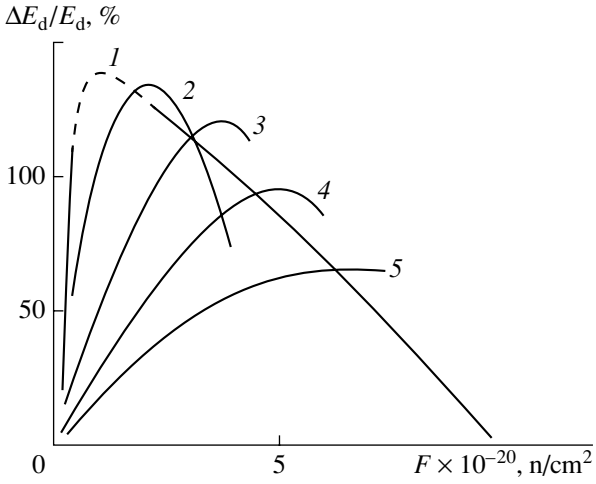

Fig. 15. Relative change in dynamic modulus of elasticity vs. neutron fluence for KUP-VM irradiated at (*1*) 50–90, (*2*) 150–200, (*3*) 300, (*4*) 450–500, and (*5*) 600–700°C.

The modulus of elasticity of nongraphitized TGN-2M was reported to drop (16%) as a result of high-fluence irradiation at 400°C [30]. At the same time, the poorly crystallized composite UPA-4 showed no modulus drop (95 and 25% after irradiation at 1100 and 1800–2000°C, respectively), presumably because of the rather good bonding between the matrix and fibers. The increase in the modulus of elasticity of nongraphitized UAM-3D was 90%.

According to Burtseva *et al.* [33], irradiation in the range 400–1000°C with fluences of $(4.1–5.7) \times 10^{21}$ n/cm^2 increases the modulus of elasticity of UAM-92-5D by 25%, in accordance with the 19–35% reported by Lebedev and Pokrovskii [30].

Irradiation at 1000°C with a fluence of 2×10^{21} n/cm^2 was reported to increase the modulus of elasticity of the 2D-reinforced composite CX 2002U

by 32% along the fibers, with no changes across the fibers [42].

The compressive strength of CCCMs typically increases by 20–50% upon irradiation and stabilizes at relatively low fluences. The strength gain decreases with increasing irradiation temperature, as in the case of graphite.

The strength gain in UAM-5D irradiated at 230–600°C with a fluence of 2×10^{20} n/cm^2 attains 50–100%. High-fluence (2×10^{21} n/cm^2) irradiation at 1000°C raises the σ_c of CX 2002U by 25–27% [42]. At the same time, at high fluences the strength of UAM-92-5D was found to decrease with increasing irradiation temperature, presumably because of oxidation [33]:

t_{irr}, °C	400	600	600	1000
$F \times 10^{-21}$, n/cm^2	4.4	4.1	7.2	5.7
$\Delta\sigma/\sigma$, %	0.05	–0.13	–0.32	–0.42

Thus, the radiation-induced changes in the physical properties of CCCMs can be understood in terms of the additive contributions from the reinforcing fibers and matrix. Also important is good adhesion between the fibers and matrix: inadequate adhesion results in cracking, thereby reducing the strength of the material.

CONCLUSIONS

The properties of CCCMs depend on

the nature of the carbon fibers (or carbon cloth) and the heat-treatment temperature,

the structure (architecture) of the reinforcing skeleton,

the nature and density of the constituent components (pitches, resins, pyrolytic carbon, or pyrolytic graphite) and their combination,

the forming process (relative amounts and sequence of components, applied pressure, and temperature), and

the nature and content of dopants (silicon or zirconium).

Neutron irradiation gives rise to anisotropic dimensional changes in CCCMs: shrinkage along the fibers and swelling across the fibers. The contribution of the fibers to these processes prevails. A more complicated architecture of CCCMs leads to more isotropic, smaller dimensional changes. In the fluence range studied (up to 10^{22} n/cm^2), no secondary swelling was detected in the samples.

The radiation-induced changes in the macroscopic properties of CCCMs are similar to those in structural carbon materials: an increase with increasing fluence, followed by stabilization at a level that is determined by the additive contributions of the fibers and matrix. Inadequate adhesion between the matrix and fibers due to the difference in the rate of size changes leads to sample bending, delamination, and microcracking, thereby reducing the strength of the material. The macroscopic properties of CCCMs and their changes under irradiation determined on small samples are underestimated owing to the disruption of reinforcement throughout the sample.

By varying the properties of CCCMs, one can tune their irradiation behavior over a wide range. In particular, increasing the heat-treatment temperature reduces dimensional changes, and reducing the density of the composite by increasing the fiber content is favorable for shrinkage of the material. Accordingly, well-graphitized silicon-doped composites with a high reinforcement level offer the highest radiation resistance.

REFERENCES

1. *Normy rascheta na prochnost' tipovykh uzlov i detalei iz grafita uran-grafitovykh kanal'nykh reaktorov* (Strength Calculations for Standard Graphite Units of Graphite–Uranium Channel Reactors), Moscow: NIKIET, NIIgrafit, IAE, ChPI, 1991.
2. Lukina, E.Yu., *Teplovoe rasshirenie uglerodnykh materialov* (Thermal Expansion of Carbon Materials), Moscow: TsNIIekonominformtsvetmet, 1990.
3. Virgil'ev, Yu.S. and Kalyagina, I.P., A Technique for Assessing the Dimensional Stability of Structural Graphite under Irradiation, *Konstr. Mater. Osn. Ugleroda*, 1978, no. 13, pp. 123–128.
4. Virgil'ev, Yu.S., Experimental Evaluation of the Radiation Resistance of Reactor Graphite, *Perspekt. Mater.*, 2000, no. 4, pp. 41–47.
5. Khabibulaev, P.K., Basic and Applied Research at the VVR-SM at the Institute of Nuclear Physics, Uzb. SSR Academy of Sciences, *At. Energ.*, 1988, vol. 64, no. 5, p. 338.
6. Karpukhin, V.I. and Nikolaenko, V.A., *Izmerenie temperatury s pomoshch'yu obluchennogo almaza* (Temperature Measurements Using Irradiated Diamond), Moscow: Atomizdat, 1971.
7. Goncharov, V.V., Burdakov, N.S., Virgil'ev, Yu.S., *et al.*, *Deistvie oblucheniya na grafit yadernykh reaktorov* (Irradiation Behavior of Reactor Graphite), Moscow: Atomizdat, 1978.
8. Konkin, A.A. and Varshavskaya, V.Ya., *Khim. Volokna*, 1974, no. 3, p. 17.
9. Andrianov, K.A., Vlasov, K.P., Kostikov, V.I., *et al.*, Potential Applications of Carbon–Carbon Composite Materials in Nuclear Power Engineering, *At. Energ.*, 1979, vol. 46, no. 6, p. 406.
10. Ponomareva, E.V. and Virgil'ev, Yu.S., Irradiation Effects on the Structure and Properties of Carbon Fibers, *Fiz. Khim. Obrab. Mater.*, 1995, no. 2, pp. 5–18.
11. Burchell, T.D., The Effects of Neutron Irradiation on the Structure and Properties of Graphite, *Proc. Mater. Specialist Meet. on Materials Data Base*, Garching, 1990.
12. Bowers, D.A. and Sopp, J.W., Carbon-Based Materials: Thermal Development Testing and Selection Process for First Wall and Divertor Applications, *Proc. 5th Int. Conf. on Fusion Reactor Materials, ICFRM-5*, Clearwater, 1991, pp. 305–308.

13. Kuznetsov, D.A., Kurolenkin, E.I., Virgil'ev, Yu.S., *et al.*, Effect of Low-Temperature (340–360°C) Neutron Irradiation on the Structure and Properties of Carbon Fibers, *Mezhdunarodnaya konferentsiya po radiatsionnomu materialovedeniyu* (Int. Conf. on the Irradiation Behavior of Materials), Alushta, 1990 (Kharkov: Khar'kov. Fiziko-Tekh. Inst., 1991, vol. 8, pp. 83–90).

14. Kurolenkin, E.I., Virgil'ev, Yu.S., and Kuznetsov, D.A., Effect of High-Temperature Neutron Irradiation on the Structure and Properties of Carbon Fibers, *Fiz. Khim. Obrab. Mater.*, 1992, no. 4, pp. 18–21.

15. Virgil'ev, Yu.S., Effect of Neutron Irradiation on the Properties of Pyrolytic Carbon, *Khim. Tverd. Topl.* (Moscow), 1993, no. 3, pp. 64–75.

16. Virgil'ev, Yu.S., Asaturov, S.A., Kurolenkin, E.I., and Makarchenko, V.G., Irradiation Effects on the Structure of Glassy Carbon, *Khim. Tverd. Topl.* (Moscow), 1992, no. 3, pp. 106–112.

17. Bullok, Irradiation Induced Dimensional Changes of Poorly Crystalline Carbon, *Carbon*, 1979, vol. 17, no. 6, pp. 447–452.

18. Virgil'ev, Yu.S. and Lebedev, I.G., Radiation Resistance of Reactor Graphites Based on Inexpensive Raw Materials, *Neorg. Mater.*, 2002, vol. 38, no. 9, pp. 1060–1064 [*Inorg. Mater.* (Engl. Transl.), vol. 38, no. 9, pp. 890–894].

19. Everett, M.R., Graphite and Matrix Materials for Very High Temperature Reactors, *Int. Conf.*, London, 1974, p. 46/1.

20. Virgil'ev, Yu.S. and Lebedev, I.G., Effect of Neutron Irradiation on Properties of Glassy Carbon, *Neorg. Mater.*, 2002, vol. 38, no. 7, pp. 810–816 [*Inorg. Mater.* (Engl. Transl.), vol. 38, no. 7, pp. 668–673].

21. Kostikov, V.I., Carbon–Carbon Composite Materials, *Zh. Vses. Khim. O–va. im. D. I. Mendeleeva*, 1989, vol. 34, no. 5, pp. 492–501.

22. Burchell, T.D., A Review of the Properties of Carbon Materials Suitable for MHTGR High-Temperature Control Rods, *ORNL/NPP-90/14*, 1991.

23. Lince, J., High Heat Flux Tests on C-Materials, *Proc. Japan–US Workshop P-92*, Nagoya, 1987, pp. 276–284.

24. *Uglerodnyi kompozit KM-5415* (Carbon Composite KM-5415), Moscow: Vneshtorgizdat, no. 6678MV, 1989.

25. *Dvukhmerno-armirovannyi uglerodnyi kompozit KUM-VM-2* (2D-Reinforced Carbon Composite KUM-VM-2), Moscow: Vneshtorgizdat, no. 6677MV, 1989.

26. Virgil'ev, Yu.S., Ponomareva, E.V., and Ponomarev, O.V., Carbon Materials for Fusion Energy Applications, *Perspekt. Mater.*, 1995, vol. 2, no. 3, pp. 218–227.

27. Virgil'ev, Yu.S., Vlasov, K.P., and Vlasov, A.K., Radiation Resistance of Carbon–Carbon Composite Materials, *At. Energ.*, 1996, vol. 80, no. 4, pp. 263–266.

28. Khanbekov, R.G., Rasulkulov, Kh.M., Virgil'ev, Yu.S., *et al.*, Resistance of Carbon–Carbon Composite Materials to High-Temperature Neutron Irradiation, *Neorg. Mater.*, 1991, vol. 27, no. 12, pp. 2664–2666.

29. Virgil'ev, Yu.S., Kalyagina, I.P., Vlasov, K.P., and Il'in, V.T., Radiation Resistance of Carbon–Carbon Composite Materials, *Neorg. Mater.*, 1992, vol. 28, no. 1, pp. 66–71.

30. Lebedev, I.G. and Pokrovskii, A.S., Radiation Testing of Carbon–Carbon Composite Materials, *Sb. Tr. GNTs RF NIIAR*, 1998, no. 4, pp. 41–53.

31. Virgil'ev, Yu.S., Irradiation Behavior of Siliconized Graphites, *Neorg. Mater.*, 1997, vol. 33, no. 6, pp. 683–690 [*Inorg. Mater.* (Engl. Transl.), vol. 33, no. 6, pp. 570–576].

32. Virgil'ev, Yu.S., Kalyagina, I.P., Rasulkulov, Kh.M., *et al.*, High-Temperature Neutron Irradiation of Carbon Materials, *Neorg. Mater.*, 1997, vol. 33, no. 5, pp. 553–561 [*Inorg. Mater.* (Engl. Transl.), vol. 33, no. 5, pp. 464–471].

33. Burtseva, T.A., Bagautdinov, R.M., Chugunov, O.K., *et al.*, The Effect of Neutron Irradiation on the Property Changes in Recrystallized Graphites and Carbon–Carbon Fiber Materials, *Mater. Specialist Meet. ICFRM-8*, Sendai, 1997.

34. Burchell, T.D., Eatherly, W.P., Robbins, J.M., and Strizak, J.P., The Effects of Neutron Irradiation on the Structure and Properties of Carbon–Carbon Composite Materials, *J. Nucl. Mater.*, 1992, nos. 191–194, p. 245.

35. Bonal, J.P., Thiele, B., Tsotridis, G., and Wu, C.H., *J. Nucl. Mater.*, 1994, nos. 212–215, p. 1218.

36. Virgil'ev, Yu.S., Ponomarev, O.V., and Ponomareva, E.V., Irradiation Behavior of Carbon-Based Composite Materials, *Neorg. Mater.*, 1996, vol. 32, no. 9, pp. 1108–1117 [*Inorg. Mater.* (Engl. Transl.), vol. 32, no. 9, pp. 971–979].

37. Virgil'ev, Yu.S. and Kurolenkin, E.I., Structural Carbon Materials for Fusion Reactor Applications and Their Radiation Resistance, *Vopr. At. Nauki Tekh., Ser.: Termoyad. Sint.*, 1992, no. 2, pp. 42–51.

38. Virgil'ev, Yu.S., Effect of Low-Temperature (50–90°C) Neutron Irradiation on Properties of Structural Graphites, *Fiz. Khim. Obrab. Mater.*, 1993, no. 3, pp. 5–16.

39. Burtseva, T.A., Chugunov, O.K., Dovguchits, E.F., *et al.*, Resistance of Carbon-Based Materials for the ITER Divertor under Different Radiation Fluxes, *Mater. Specialist Meet. ICFRM-5*, Clearwater, 1991.

40. Wu, C.H., Bonal, J.P., Thiele, B., *et al.*, Neutron Irradiation Effects on the Properties of Carbon Materials, *J. Nucl. Mater.*, 1994, nos. 212–215, pp. 416–420.

41. Virgil'ev, Yu.S., *Reaktornyi grafit i ego svoistva* (Reactor Graphite and Its Properties), Moscow: TsNIIekonominformtsvetmet, 1990.

42. Eto, M., Ishyama, S., Ugachi, H., *et al.*, *J. Nucl. Mater.*, 1994, nos. 212–215, p. 1223.